Step-scheme mechanism in NiO/CdS heterojunction nanoarray for visible light-activated gas sensing at room temperature

Wufei Gong, [a] Shenman Yao, [a] Dehua Wang, [a] Jiahao Li, [a] Yulin Zhu, [a] Jianxian You,

[a] Yan Liang, [b], Yanxing Yang, [c] and Yong Yang [a],**

[a] Jiangxi Key Laboratory of Nanomaterials and Sensors, Jiangxi Key Laboratory of

Photoelectronics and Telecommunication, School of Physics, Communication and

Electronics, Jiangxi Normal University, Nanchang 330022, Jiangxi, P.R. China

[b] Department of Artificial Intelligence, Nanchang Key Laboratory of New Electronic

Components and Sensing Technology, Jiangxi University of Technology, Nanchang

330098, Jiangxi, P.R. China

[c] Department of Chemistry and Chemical Biology, Rutgers University, Piscataway,

New Jersey 08854, United States

Experimental

1. Materials preparation

All the reagents were purchased from Aladdin Reagent Co. Ltd., which are analytical grade and used without further purification. The commercial alumina flats which had been coated with Pt-interdigitated electrodes (produced by Huachuang Ruike Science and Technology Co. Ltd.) were washed with deionized water and ethanol alternately before use.

1.1. Preparation of NiO nanosheets array

Firstly, 1.1632 g of $Ni(NO_3)_2 \cdot 6H_2O$, 0.592 g of ammonium fluoride and 1.2 g of urea were dissolved sequentially in 72 mL of deionized water under strong stirring. After fully mixing, the transparent solution with green color and cleaned commercial alumina flats were transferred to a 100 mL Teflon reactor. The reactor was sealed with a stainless steel autoclave and put into the oven. After the reaction at 100 °C for 8 h, the reactor was naturally cooled to ambient temperature. The commercial alumina flat with NiO precursors deposited on it was washed with deionized water and ethanol for several times, and dried at 60 °C for 12 h. The NiO nanosheets array was obtained by calcining NiO precursors deposited on commercial alumina flats at 500 °C for 2 h.

1.2. Preparation of S-scheme NiO/CdS heterojunction nanoarray

CdS nanoparticles were further grown on the surface of NiO nanosheets array by a mixed solvothermal method to obtain the S-scheme NiO/CdS heterojunction nanoarray. Typically, 11 mg of $Cd(CH_3COO)_2 \cdot 2H_2O$, 3 mg of thiourea were dissolved in 20 mL mixed solvent of deionized water and ethylene glycol (the volume ratio of deionized water and ethylene glycol was 1:1) to obtain the reaction solution under strong stirring. The reaction solution was transferred to a 50 mL Teflon reactor,

and then the alumina flat with NiO nanosheets array was immersed into the reaction solution. The reactor was sealed with a stainless steel autoclave and put into the electric oven. The reaction temperature was set to 170 °C and the reaction time was 20 h. After the reactor was naturally cooled to ambient temperature, the alumina flat with S-scheme NiO/CdS heterojunction nanoarray deposited on it was washed with deionized water and ethanol for several times, and dried at 60 °C for 12 h. The product was denoted as NiO/CdS-1. For comparison, the amount of $Cd(CH_3COO)_2 \cdot 2H_2O$ and thiourea was increased to 5 times with other reaction process unchanged, and the obtained product was denoted as NiO/CdS-2. For comparison, pure CdS nanoparticles were obtained by the same procedure. In order to conduct a more in-depth and systematic study of the effect of CdS concentration in the gas sensing properties, another two types of NiO/CdS heterojunctions with theoretical CdS concentrations half and twice that of NiO/CdS-1 (referred to as NiO/CdS-1-0.5 and NiO/CdS-1-2, respectively) were further synthesized.

2. Materials characterization

X-Ray diffraction patterns (XRD) measurement was conducted on a Malvern Panalytical X-ray diffractometer. Scanning electron microscopy (SEM) and transmission electron microscopy (TEM) images were recorded by a ZEISSEVO microscope and JEM-2100 microscope, respectively. X-ray photoelectron spectroscopy (XPS) analysis was conducted on a Thermo Fisher Scientific spectrometer (Escalab 250Xi) which was employed with Al Kα radiation. Nitrogen

adsorption-desorption measurement was conducted by a BET analyzer (Micro for TriStar II Plus 2.02) at 77 k. UV-Vis absorption spectra were obtained using a U-3310 UV-Vis spectrometer by Hitachi. Mott-Schottky plot was measured by a CHI 660E electrochemical work station with a potential step of 5 mV. Electron spin resonance (ESR) measurement was conducted on EMXPlus spectrometer. Photoluminescence (PL) spectra were carried out with a Fluoro MAX-4 spectrometer by HORIBA Jobin Yvon, and the excitation wave length was 325 nm. The photocurrent measurement were carried on a CHI 760D electrochemical work station in standard three-electrode system. Pt plate and Ag/AgCl were used as counter electrode and reference electrode, respectively. The working electrode was obtained by drop casting 0.4 mL of the slurry of gas sensing materials powder (concentration: 6 mg/mL) onto ITO substrate, and then dried at 60 °C in vacuum. 0.5 M Na_2SO_3 aqueous solution was used as electrolytes for measurement. A Xe lamp with a power of 500 W was employed as light source.

3. Measurement of gas sensing performance

Since the above semiconductor materials are in-situ grown on the surface of commercial alumina flat which had been coated with Pt-interdigitated electrodes in the form of nanoarrays, the gas sensing characteristics can be tested directly with a commercial four channel gas sensing tester. During the tests, white LED light with low power (0.06 W, the light intensity is 1.324 $\mu W/cm^2$) was used to illuminate the sensor, target gases were injected into the test chamber, and then the chamber was lifted to introduce ambient air. The room temperature in all gas sensing tests

referred to 25 °C, which was accurately controlled through Labview software. The gas sensing response was defined as the resistance ratio in air and target gas (R_a/R_g or R_g/R_a).

4. Method of calculation

The present first principle DFT calculations are performed by Vienna Ab initio Simulation Package (VASP) with the projector augmented wave (PAW) method.[1,2] The exchange-functional is treated using the generalized gradient approximation (GGA) of Perdew-Burke-Emzerhof (PBE) functional.[3] The energy cutoff for the plane wave basis expansion was set to 450 eV and the force on each atom less than 0.05 eV/Å was set for convergence criterion of geometry relaxation. Grimme' s DFT-D3 methodology was used to describe the dispersion interactions.[4] Partial occupancies of the Kohn−Sham orbitals were allowed using the Gaussian smearing method and a width of 0.05 eV. The Brillourin zone was sampled with Monkhorst mesh $2\times2\times1$ through all the computational process. The self-consistent calculations apply a convergence energy threshold of 10^{-5} eV. A 15 Å vacuum space along the z direction was added to avoid the interaction between the two neighboring images.

The adsorption energy (Eads) of adsorbate molecule was defined as

$$E_{ads} = E_{mol/surf} - E_{surf} - E_{mol(g)}$$

where $E_{mol/surf}$, E_{surf} and $E_{mol(g)}$ are the energy of adsorbate molecule adsorbed on the surface, the energy of clean surface, and the energy of isolated molecule in a cubic periodic box, respectively.

Reference

[1] G.Kresse, J. Furthmüller, Efficiency of ab-initio total energy calculations for metals and semiconductors using a plane-wave basis set, Comp. Mater. Sci. 6 (1996) 15–50.

[2] P.E. Blöchl, Projector augmented-wave method, Phys. Rev. B 501 (1994) 17953–17979.

[3] J.P. Perdew, J.A. Chevary, S.H. Vosko, K.A. Jackson, M.R. Pederson, D.J. Singh, C. Fiolhais, Atoms, molecules, solids, and surfaces: Applications of the generalized gradient approximation for exchange and correlation, Phys. Rev. B 46 (1992) 6671–6687.

[4] S. Grimme, J. Antony, S. Ehrlich, H. Krieg, A consistent and accurate ab initio parametrization of density functional dispersion correction (DFT-D) for the 94 elements H-Pu, J. Chem. Phys. 132 (2010) 154104.
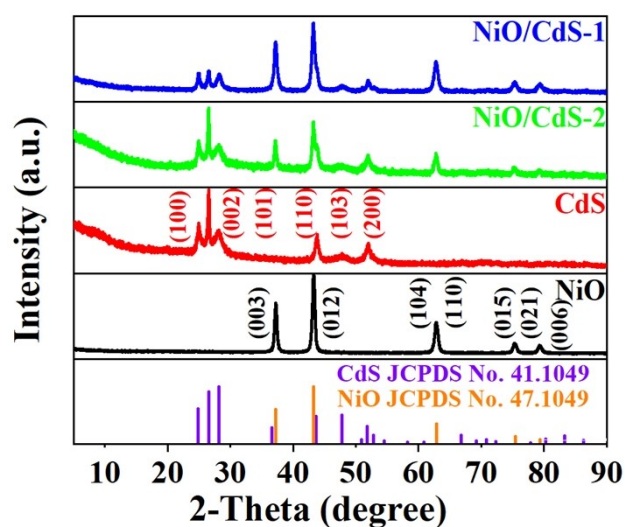
Fig. S1. XRD patterns of the different samples.
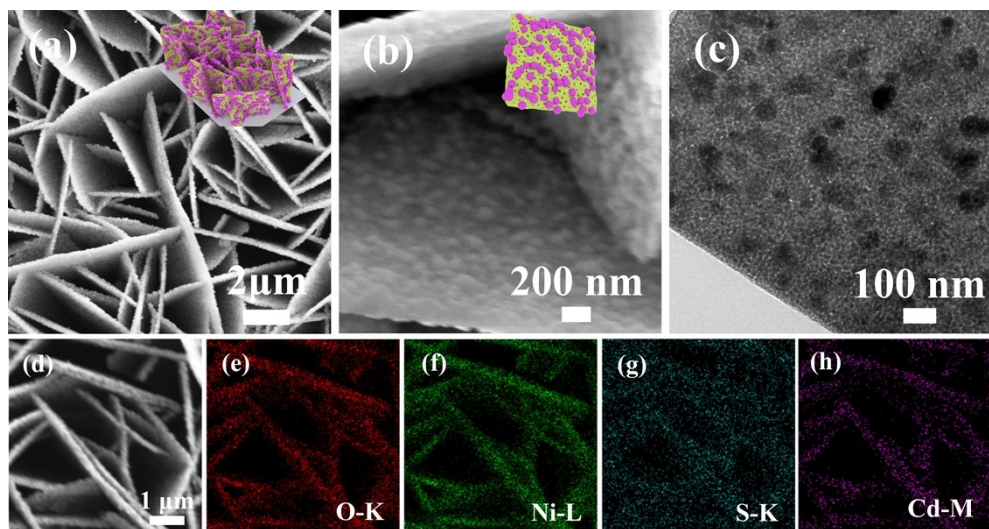
Fig. S2. (a)-(c) SEM and TEM images of NiO/CdS-2 heterojunction nanoarray, inset in (a) and (b) are the corresponding schematic images; (d)-(h) Elemental mapping images of NiO/CdS-2 heterojunction nanoarray.
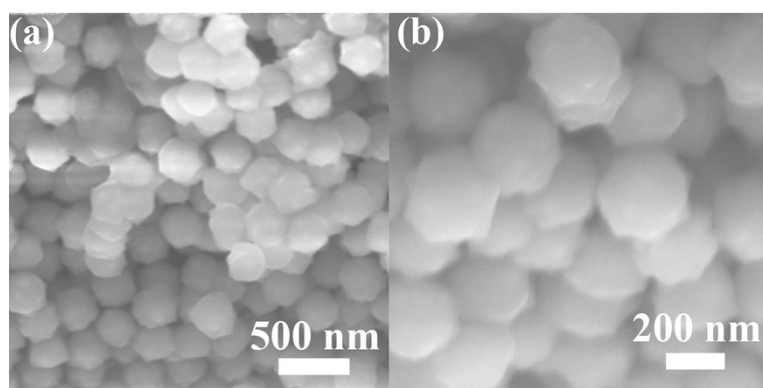
Fig. S3. (a)-(b) SEM images of pure CdS nanoparticles.
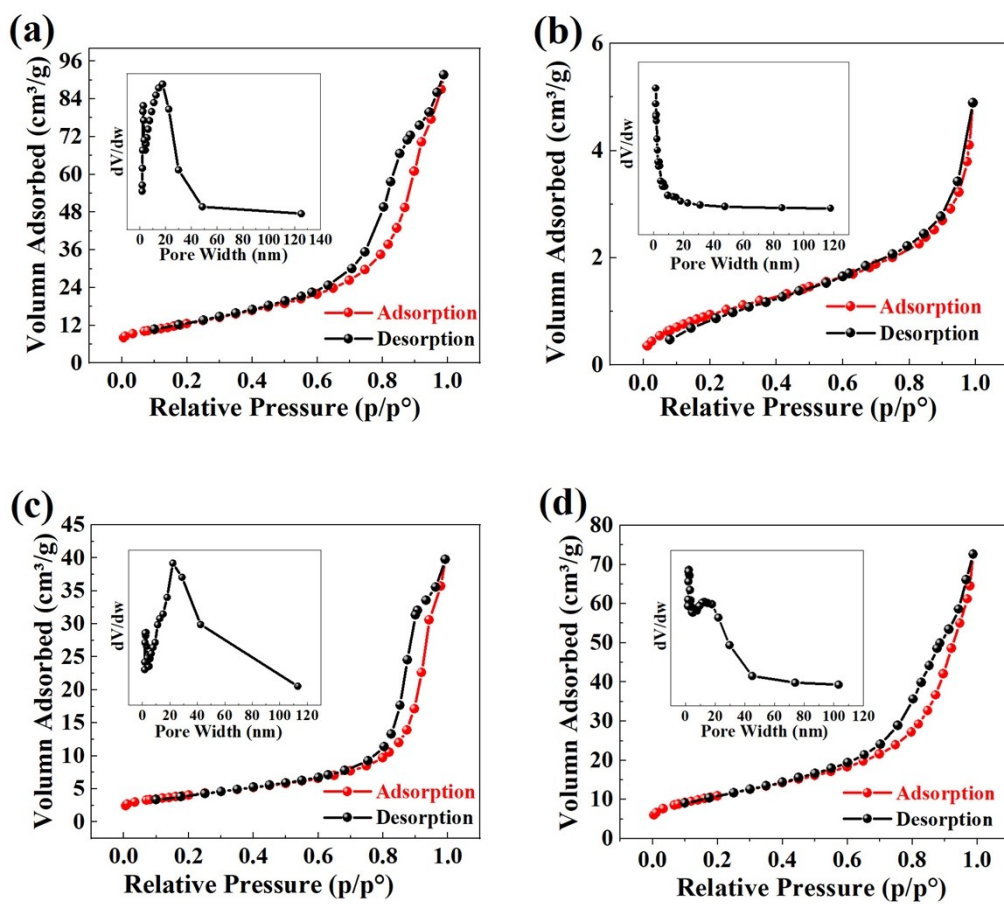
Fig. S4. Nitrogen adsorption-desorption isotherm of (a) NiO, (b) CdS, (c) NiO/CdS-2 and (d) NiO/CdS-1. Inset are the corresponding pore width distribution curves.

Table S1. structural parameters of different samples as probed by N_2 adsorption-desorption isotherms.

Samples	NiO	CdS	NiO/CdS-1	NiO/CdS-2
BET surface area (m²/g)	44.25	3.79	39.72	14.04
Pore volume (cm³/g)	0.14	0.007	0.11	0.06
Average pore width (nm)	12.46	7.96	11.31	16.96
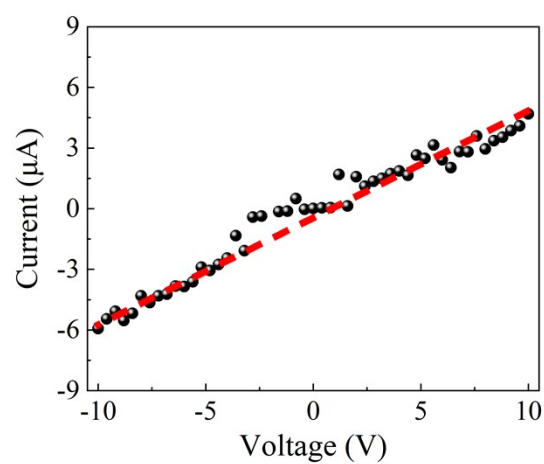
Fig. S5. I-V characteristics between the two neighboring electrodes bridged by the NiO nanosheets array.
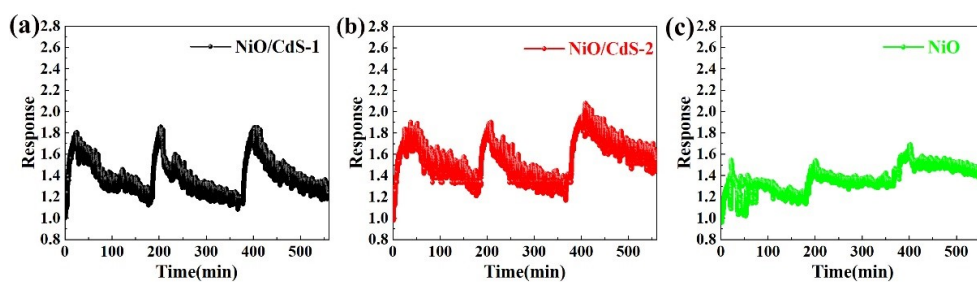
Fig. S6. Room temperature sensing performance of the different samples toward 100 ppm triethylamine without light activation.

Fig. S7. The resistance vs time for the NiO/CdS-1 nanoarrays under both the dark and visible light illumination with the presence of triethylamine.

Fig. S8. Relationship of logarithmic response values versus triethylamine concentration.
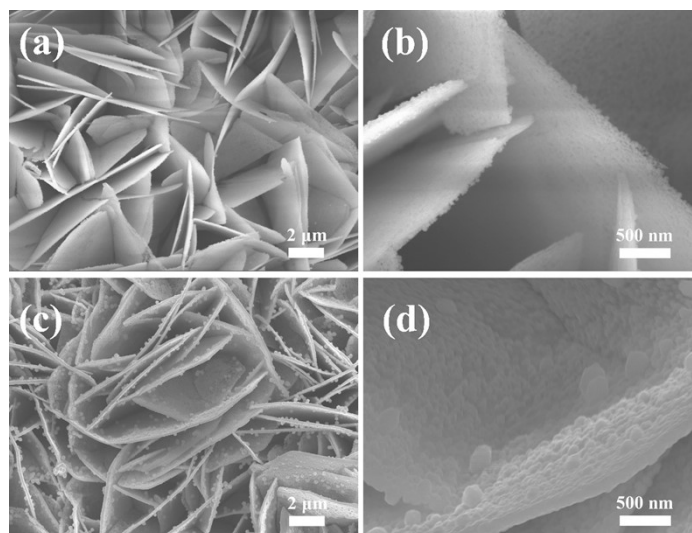
Fig. S9. SEM images of the NiO/CdS heterojunction with different CdS loading concentrations: (a) and (b) NiO/CdS-1-0.5; (c) and (d) NiO/CdS-1-3.
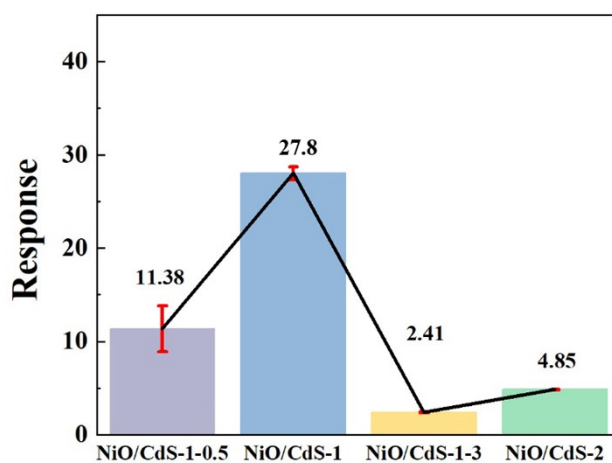
Fig. S10. Comparison of response values of the NiO/CdS heterojunction with different CdS loading concentrations towards 100 ppm triethylamine.

Table S2. Comparison of specific surface area and response value of different NiO/CdS heterojunction towards 100 ppm triethylamine.

Sensing materials	S_{BET}	Response	Response per specific
	(m^2/g)	(R_a/R_g)	surface area
NiO/CdS-1	39.72	27.8	0.699
NiO/CdS-2	14.04	5.1	0.363

Table S3. Performance comparison of the S-scheme NiO/CdS-1 heterojunction nanoarray with various related triethylamine sensors.

Gas sensing materials	Concentration (ppm)	Response value (R_a/R_g, R_g/R_a)	Operating temperature (°C)	Reference
S-scheme NiO/CdS heterojunction	10 100	4.9 27.8	25	This study
Sn doped NiO hollow nanofibers	100	16.6	180	*Sensor. Actuat. B. Chem. 340 (2021) 129971*
Sn doped NiO nanoparticles	100	8.2	260	*Inorg. Chem. Commun. 136 (2022) 109104*
NiO-BN p-n heterojunction	500	23.8	300	*Adv. Powder Technol. 32 (2021) 3801–3813*
Fe_2O_3@NiO(CuO) core-shell nanorods	50	13.5	40	*Sensor. Actuat. B. Chem. 245 (2017) 375–385*
CdS QDs on ZnO porous microrods	50	9.87	160	*Vacuum 212 (2023) 112003*
0D/2D CdS/ZnO	50	20	200	*J. Colloid Interface Sci. 600 (2021) 898–909*
V_2CT_x	500	3.25%	25	*ACS Appl. Nano Mater. 4(2021) 6257-6268*
$SnS_2/Ti_3C_2T_x$	50	38%	25	*Sensor. Actuat. B. Chem. 381 (2023) 133360*
Fe_2O_3 nanosheets	100	17	300	*Langmuir 33 (2017) 8671–8678*
porous $NiCo_2O_4$ nanoplate	10 100	2.58 3.25	220	*Sensor. Actuat. B. Chem. 323 (2020) 128663*
Hollow $GaFeO_3$ microcubes	200	7.4	200	*Ceram. Int. 46 (2022) 18675−18682.*
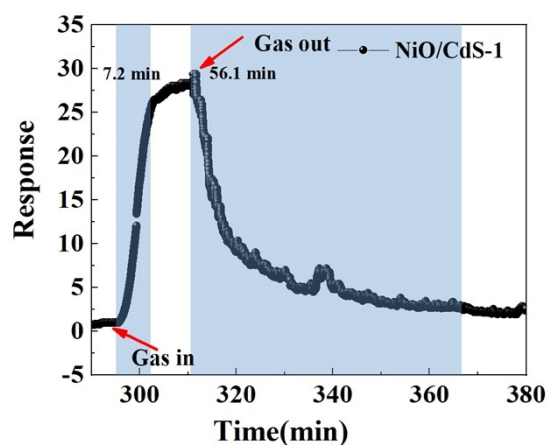
Fig. S11. Response and recovery of NiO/CdS-1 to 100 ppm triethylamine.
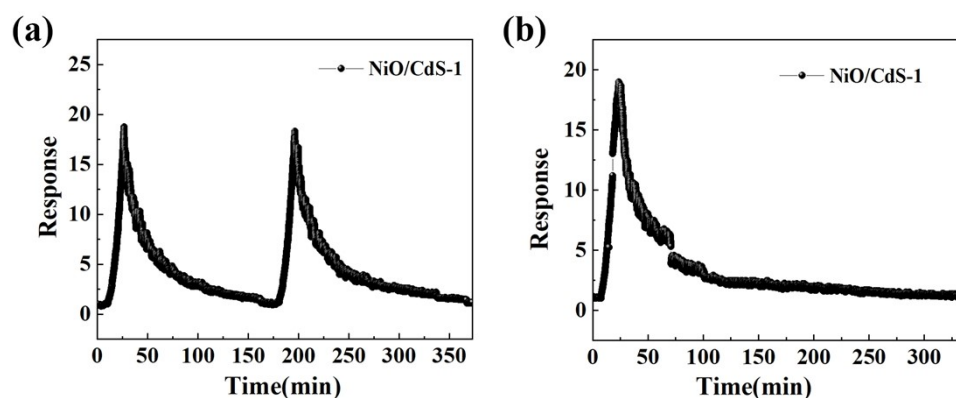
Fig. S12. Sensing properties of NiO/CdS-1 heterojunction nanoarray towards 100 ppm triethylamine under high humidity condition. (a): 84% (b): 93%.
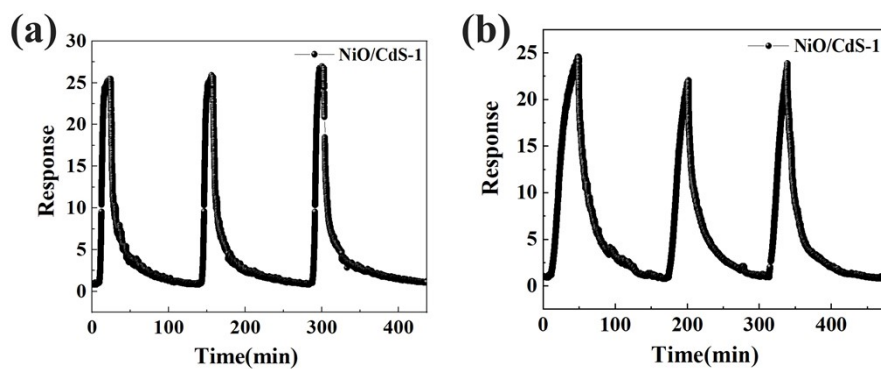

Fig. S13. Sensing properties of NiO/CdS-1 heterojunction nanoarray towards 100 ppm triethylamine after (a) 13 days and (b) 535 days.
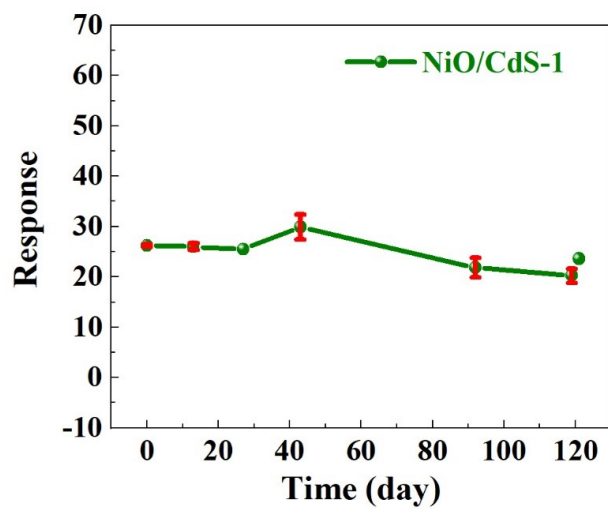
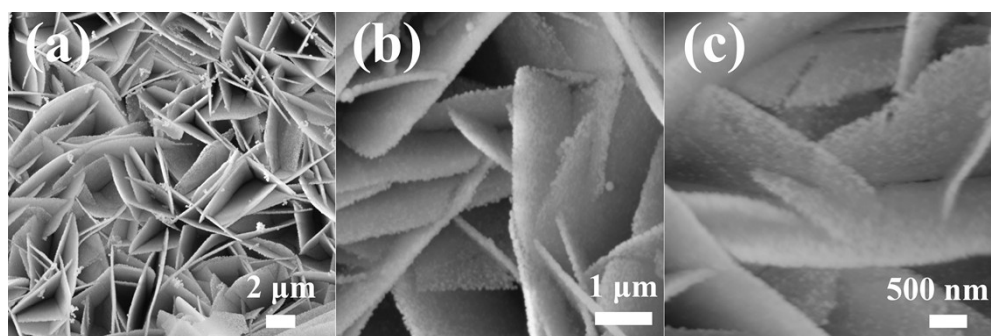**Fig. S14**. Long-term stability tests of the response value of NiO/CdS-1 heterojunction nanoarray towards 100 ppm triethylamine.

Fig. S15. SEM images of NiO/CdS-1 heterojunction nanoarray after long-term using (551 days).
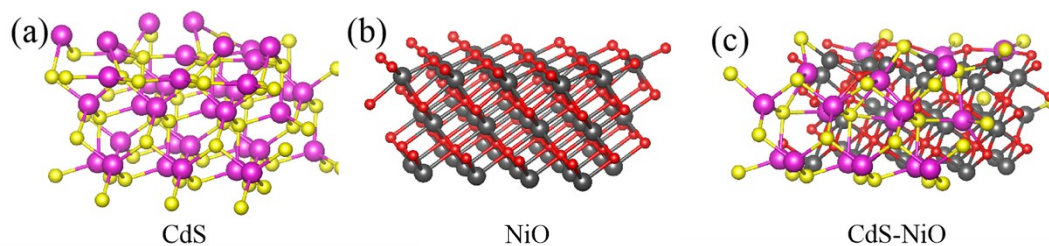
Fig. S16. The atomic configuration of different structure.
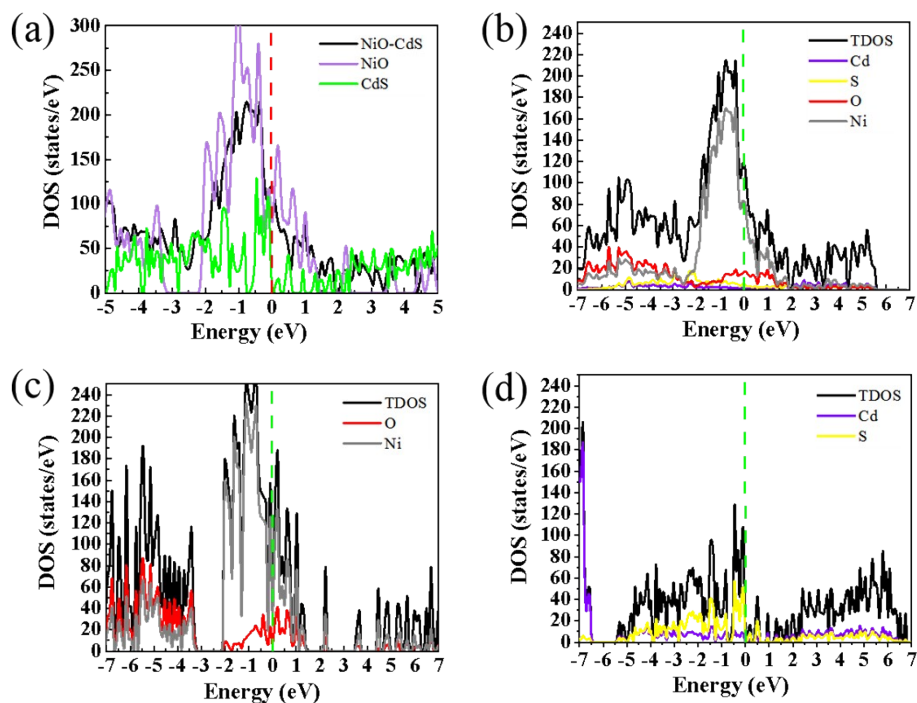
Fig. S17. (a) Total density of states of the different samples. Detailed density of states of (b) NiO/CdS heterojunction, (c) NiO and (d) CdS.
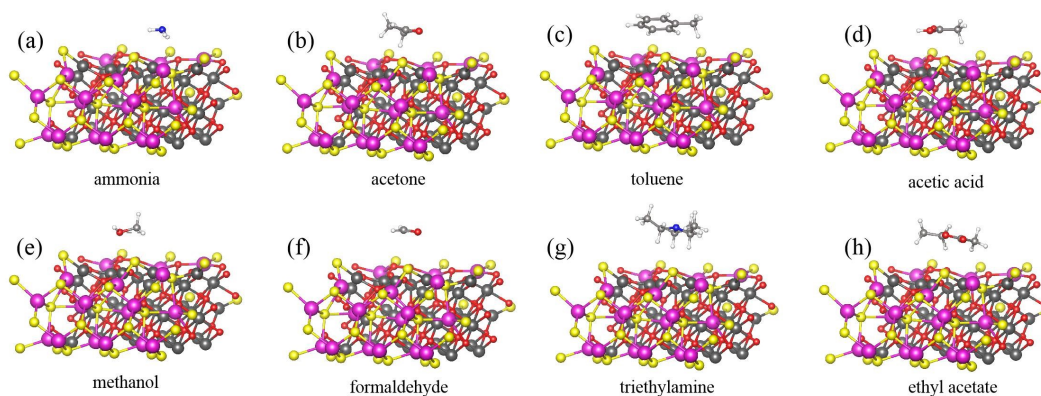
Fig. S18. The adsorption configurations for different gas molecules on the surface of NiO/CdS heterojunction.

Adsorption energy (eV)
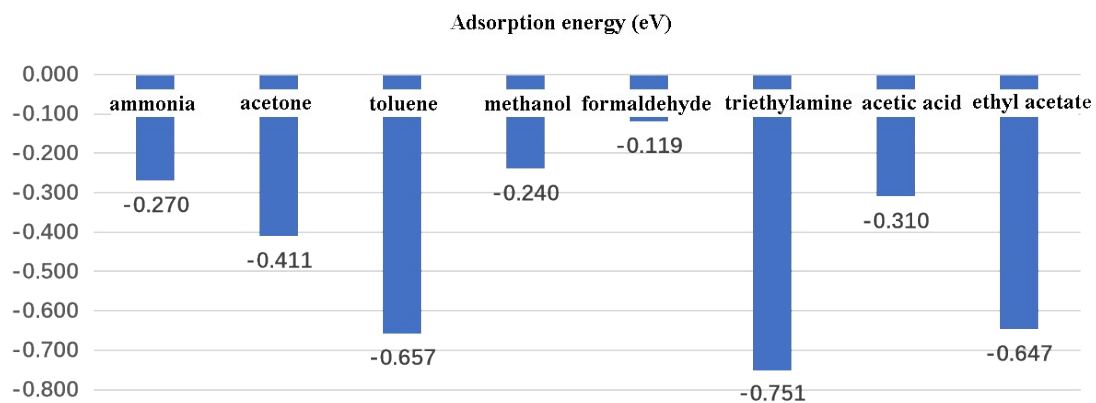
Fig. S19. The adsorption energies of different VOCs gas molecules on the surface of NiO/CdS heterojunction.
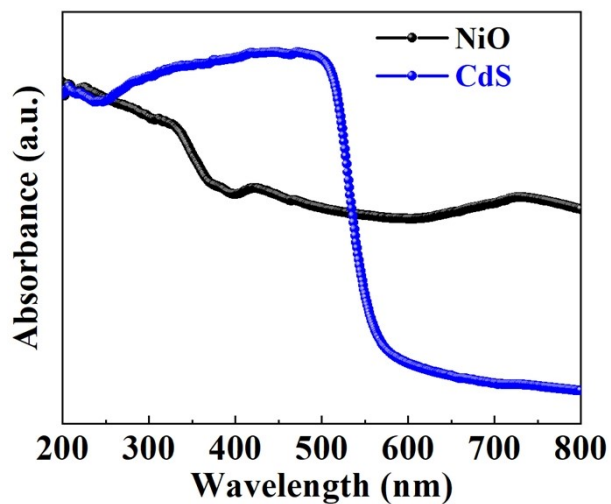
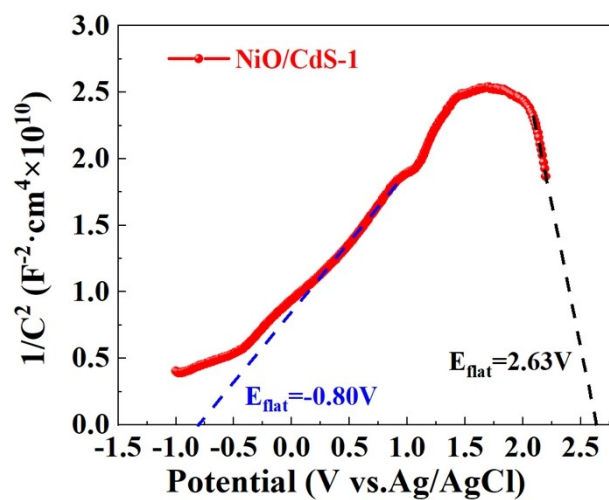**Fig. S20**. UV-Visual absorption spectra of the different samples.

Fig. S21. Mott-Schottky plots of NiO/CdS-1 heterojunction nanoarray.
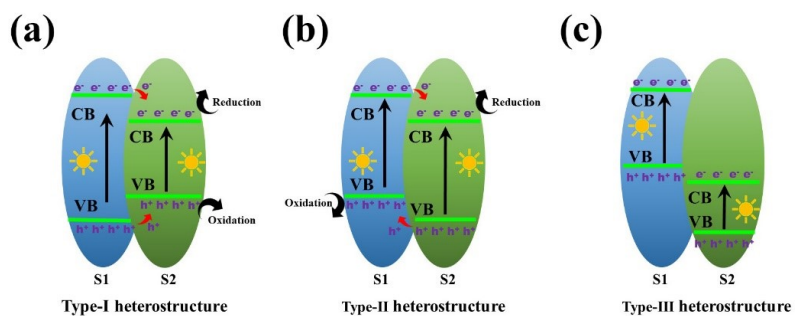
Fig. S22. Schematic illustration of the charge transfer and separation process in traditional semiconductor heterojunctions: (a) type I, (b) type II and (c) type III.
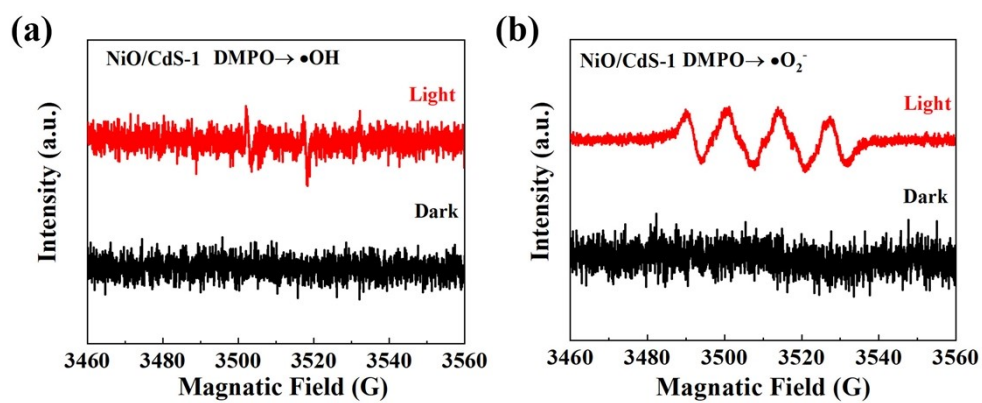
Fig. S23. ESR spectra of NiO/CdS-1 heterojunction nanoarray for (a) DMPO-・OH and (b) DMPO-・O_2^-.
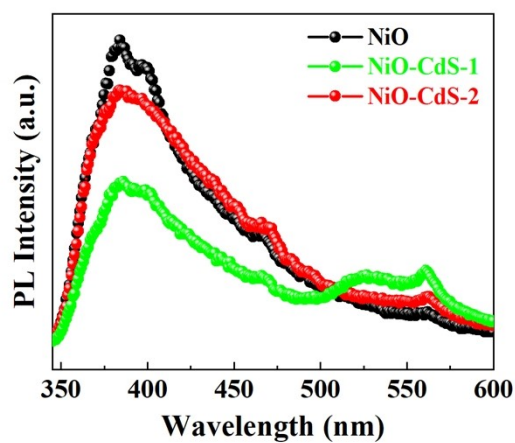

Fig. S24. PL spectra of the different samples.
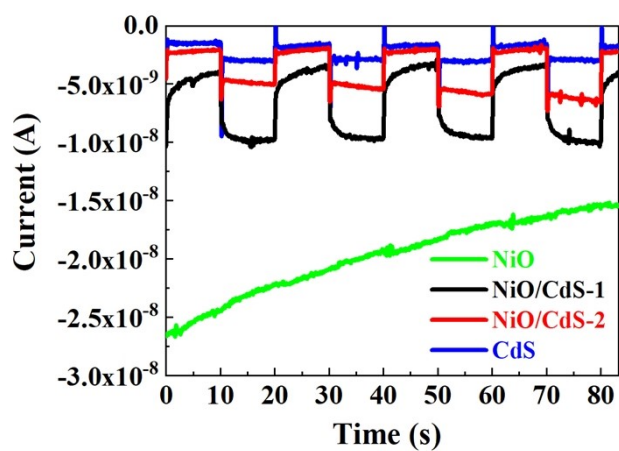

Fig. S25. Transient photo-current responses of the different samples.
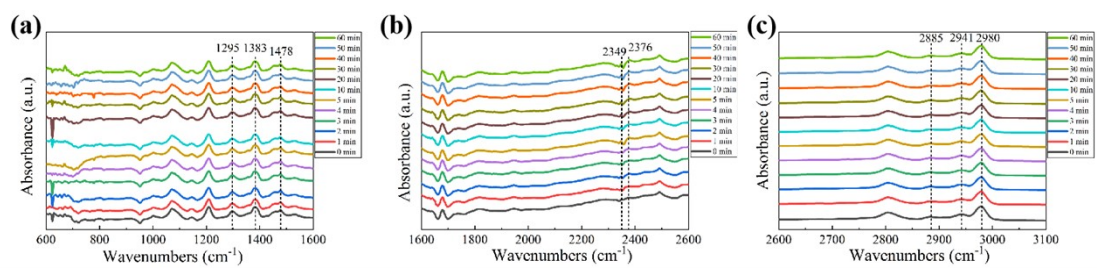
Fig. S26. In-situ Fourier transform infrared spectroscopy of NiO/CdS-1 heterojunction nanoarray in triethylamine atmosphere.